第 33 卷第 3 期
2017 年 3 月

无 机 化 学 学 报
CHINESE JOURNAL OF INORGANIC CHEMISTRY

Vol.33 No.3
509-518

ZnO/BiOI 微球的合成及其光催化性能

王元有* 龚爱琴 余文华
(扬州工业职业技术学院,扬州 225127)

摘要: 通过一步溶剂热法合成 ZnO/BiOI 纳米复合材料,在 $Bi(NO_{3})_{3}\cdot 6H_2O$、KI、ZnO 和乙二醇(EG)溶剂中,制备出的样品尺寸和形貌采用 X 射线粉末衍射(XRD)、场发射扫描电镜(FESEM)、高分辨透射电镜(HRTEM)、紫外-可见漫反射光谱(DRS)、X 射线光电子能谱(XPS)、N_2 吸附-脱附等,对实验所得产物的组成、结构及光学性质等进行表征。以染料罗丹明 B(RhB)水溶液和气态乙醛作为降解对象,采用 BiOI、ZnO/BiOI 和 ZnO 微纳材料作为光催化剂,通过对 BiOI、ZnO/BiOI 和 ZnO 微纳材料在可见光下光催化降解染料罗丹明 B(RhB)水溶液和气态乙醛,结果表明多孔微纳材料的 ZnO/BiOI 具有更高的降解效率,实验表明多孔微纳材料的 ZnO/BiOI 具有更高的氧空位浓度,因此使其催化活性增强,讨论了其可能的催化活性机理。

关键词: ZnO/BiOI 纳米复合材料; 光催化; 乙醛
中图分类号: O643 **文献标识码**: A **文章编号**: 1001-4861(2017)03-0509-10
DOI:10.11862/CJIC.2017.061

Synthesis and Photocatalytic Characterization of ZnO/BiOI Microspheres

WANG Yuan-You* GONG Ai-Qing YU Wen-Hua
(*Department of Chemical Engineering, Yangzhou Polytechnic Institute, Yangzhou, Jiangsu* 225127, *China*)

Abstract: Porous ZnO/BiOI microspheres composed of ultrathin nanosheets were successfully fabricated by an ethylene glycol-assisted solvothermal method, The morphology and size of the as-prepared samples were characterized by X-ray powder diffraction (XRD), field emission scanning electron microscopy (FESEM), high resolution transmission electron microscopy (HRTEM), UV-Vis diffuse reflectance spectra (DRS), X-ray photoelectron spectroscopy (XPS) and N_2 adsorpion-desorption measurements. The photocatalytic degradation of RhB aqueous solution shows that the porous ZnO/BiOI microspheres have the highest photodegradation performance with visible light and acetaldehyde (CH_3CHO) gas degradation.This finding indicates that the heterojunction effect created between two different semiconductors is of importance in determining the dynamic properties of photogenerated charge transfer and the related photocatalytic properties.

Keywords: Porous ZnO/BiOI microspheres; photocatalytic; acetaldehyde

0 Introduction

With the rapid development of industry, an enormous amount of industrial dyes, volatile organic compounds (VOCs) are hazardous pollutants emitted from paints, solvents, preservatives,automobile exhaust gas, industrial facilities, and so on. VOCs also have brought serious threats to our health. Among the various techniques for effective removal of indoor air pollutant of VOCs, photocatalytic oxidation, as an environmental friendly technology, has attracted much attention for its potential application in utilizing the

收稿日期:2016-11-08。收修改稿日期:2016-12-30。
国家自然科学基金(No.21505118),江苏省自然科学基金(No.BK2150438),江苏省“青蓝工程”(No.2016-15)和扬州工业职业技术学院重点科研项目(No.2016xjzk001)资助。
*通信联系人。E-mail:wangyy@ypi.edu.cn

cheap and abundant solar energy. Increasing attention has been paid to the degradation of industrial dyes as well as VOCs. ZnO is one of the most promising candidates for the degradation of organic pollutants because of its low cost, environmental friendliness and wide band gap (3.37 eV)[1-3]. A copious amount of studies have been conducted on the synthesis and photocatalytic testing of ZnO nanocrystals for the degradation of organic pollutants both in aqueous solution and gaseous phase[4-13]. However, the quick recombination of the photo-excited electrons and holes in ZnO always lead to the reduction of photocatalytic efficiency. One of the methods to increase the efficiency of the photocatalytic activity is to develop heterogeneous metal/semiconductor nanocomposite materials. ZnO coupling with metal oxide is one of the basic methods of affecting their optical response and photochemical activity. A lot of reports of ZnO coupling with metal oxide heterostructures can be found. For such composites, metal oxide can act as introducing states in the band gap. Metal oxide acts as electron collector and produces heterojunctions with ZnO , it also extends its optical response into the visible range.

A lot of semiconductors have been applied in photocatalytic for formaldehyde degradation, such as ZnO, CeO_2, Ta_2O_5, $InVO_4$, MnO_2, TiO_2, and Bi_2O_3 [14-22]. Among these photocatalysts, TiO_2 photocatalyst has attracted much interest because of its high effectiveness, stability and nontoxicity. TiO_2 can decompose formaldehyde to a harmless compounds by UV light energy over its band-gap energy (3.2 eV) resulting in the generation of mobile electrons in the higher energy, conduction band and positive holes in the lower energy, valence band. The radicals take the electron from the nearby formaldehyde to become stable oneself. In this way, the formaldehyde is decomposed by loss of electron and finally becomes CO_2 and H_2O. However, as a wide band gap semiconducting material, titanium dioxide responds only in the ultraviolet (UV). The use for morphology and size-controlled metal, the metal oxide composites and different ionic doping are the three most commonly utilized methods for enhancing the photocatalytic properties of ZnO-based materials. But to the best of our knowledge, the reports on porous ZnO/BiOI microspheres and their photocatalytic activity of ZnO/BiOI microspheres under visible light irradiation are scarce up to now.

A study of a more complicated system will provide deeper insight into the development of a more practical catalyst applicable to a real contaminated target. The obtained ZnO/BiOI heterojunctions show remarkably enhanced photocatalytic performances for acetaldehyde degradation in aqueous solution under simulated solar light irradiation, which are higher than those of pure BiOI and ZnO materials. Furthermore, the photocatalytic activity enhancement mechanism of the ZnO/BiOI heterojunctions and the process of charge separation and transfer at the surface or interface were also discussed.

Herein, we report a facile and feasible approach to prepare ZnO/BiOI microspheres structure by a simple template-free hydrothermal technique using the simple inorganic salts $Zn(NO_3)_2 \cdot 6H_2O$, $Bi(NO_3)_3 \cdot 5H_2O$ and KI as original materials. for the first time.

1 Experimental

1.1 Materials

Chemicals: $Bi(NO_3)_3 \cdot 5H_2O$, $Zn(NO_3)_2 \cdot 6H_2O$, KI, rhodamine B (RhB), aceteldehyde (CH_3CHO), ethanol (C_2H_5OH) and cinnamate were purchased from Sinopharm Chemical Reagent Co., Ltd. (Shanghai, China) and used without further purification. All chemicals used in this study were of commercially available analytical grade.

1.2 Preparation of the ZnO/BiOI microspheres

ZnO/BiOI microspheres were synthesized by a facile method . Typically, ZnO microspheres were prepared according to the protocol as our previous report[23], ZnO was added to 15 mL of ethylene glycol containing a stoichiometric amount of $Bi(NO_3)_3 \cdot 5H_2O$ ($n_{Zn}/n_{Bi}=1$) with constant stirring, white precipitates formed. Then, a stoichiometric amount of KI was added, and the mixture was stirred for 30 min at room temperature. The mixture was magnetically stirred at

room temperature for 30 min and then transferred to a 25 mL Teflon-coated steel autoclave. The autoclave temperature was raised to 160 ℃. Reactions were stopped at 12 h. The precipitates were collected, washed thoroughly with deionized water and ethanol, and dried at 50 ℃ in air. For comparison, subsequently, different stoichiometric amounts of $Bi(NO_3)_3 \cdot 5H_2O$ were added to the resultant mixed solution. The Bi/Zn molar ratios were kept to 0, 1:1, 1:2, 1:3, and 1:5 (denoted as ZnO, ZB-1, ZB-2, ZB-3, and ZB-5).

1.3 Characterization

The phase purity of the products was characterized by X-ray diffraction (XRD, German Bruker AXSD8 ADVANCE X-ray diffractometer) using a X-ray diffractometer with Cu $K\alpha$ radiation(λ= 0.154 18 nm, U=40 kV, I=40 mA). Morphology information of the as-prepared particles was obtained on a Japan Hitachi S-4800 field emission scanning electron microscope (SEM). Transmission electron microscope (TEM) images, high resolution transmission electron microscopy (HRTEM) images, high angle annular dark field (HAADF) images and elemental mapping images were obtained on an American FEI Tecnai G2 F30 S-TWIN field-emission transmission electron microscopy (operated at 300 kV). Diffuse reflectance spectra (DRS) were measured using a UV-Vis spectrophotometer (Shimadzu,UV-2600) equipped with an integrating sphere unit (Shimadzu,ISR-2600 Plus). Fluorescence spectra were obtained using a photoluminescence spectrometer (JASCO, FP-8500). X-ray photoelectron spectra (XPS) were recorded on a ESCALAB 250Xi system (Thermo Scientific).

1.4 Photocatalytic testing

RhB aqueous solution photodegradation evaluation test: the photocatalytic activities of as-prepared products were tested by degrading an organic dye, RhB in aqueous solution. In the photocatalytic experiments, 20 mg as-synthesized nanocrystals were added into a bottle which contains 100 mL RhB aqueous solution (5×10^{-5} mol·L^{-1}), and the solution was stirred in the dark for 30 min to reach adsorption-desorption equilibrium between the catalyst and RhB. Then, the mixture was irradiated by an 250 W Xe lamp. After the mixture was irradiated for a given time, then about 3 mL was taken out and immediately centrifuged. The degradation of RhB was monitored by measuring the absorbance of the solution using a Cary 5000 UV-Vis spectrophotometer.

CH_3CHO gaseous phase photodegradation evaluation test: 0.1 g samples were spread on the bottom of a watch-glass. The watch-glass was put and then 125 mL acetaldehyde / pure air mixture gases (550 μL·L^{-1}) were injected into the Tedlar bag (Polyvinyl fluoride, As ONE Co. Ltd). The bag was located in dark room for 2 h to ensure the adsorption equilibrium. Then the samples were irradiated under LED lamp (central wavelength of 365 nm) with 1 mW·cm^{-2} light intensity. The concentration variation of acetaldehyde and CO_2 evolution were monitored by on-line gas chromatography (Agilent Technologies, 3000A Micro-GC, TCD detector) equipped with OV1 and PLOT-Q columns.

2 Results and discussion

2.1 XRD curves and BET tests of as-synthesized samples

Fig.1 shows X-ray diffraction (XRD) patterns of pure BiOI, pure ZnO, and ZnO/BiOI microspheres. All of the diffraction peaks shown in spectra a and e of Fig.1 can be indexed to the tetragonal phase of BiOI (JCPDS card 73-2062) and the hexagonal phase of

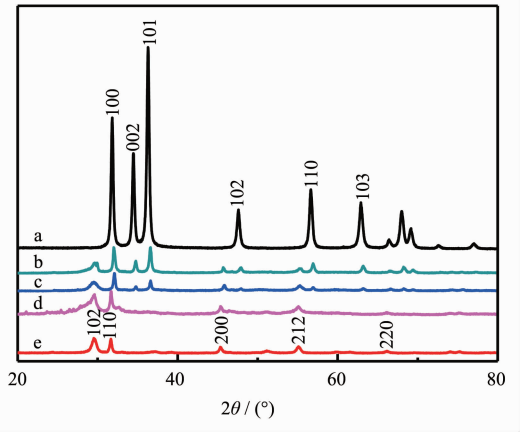

a: ZnO; b: ZB-1; c: ZB-3; d: ZB-5; e: BiOI

Fig.1 XRD patterns of ZnO,ZnO-BiOI microspheres and BiOI

ZnO (JCPDS card 36-1451), respectively. The diffraction peaks of both BiOI and ZnO were sharp and intense, which indicated their highly crystalline nature. No impurity peaks were observed,those conrmed the high purity of the two products. Two sets of XRD peaks of tetragonal BiOI and hexagonal ZnO can be clearly observed in Fig.1(b,e). Meanwhile, the diffraction peaks corresponding to ZnO and the diffraction peak intensity ratio (IZnO, (100)/IBiOI, (102)) between the two components decrease gradually with increasing Bi/Zn molar ratio. Notably, the diffraction peaks assigned to BiOI in the patterns of ZnO/BiOI microspheres became broader and weaker, which suggested that the presence of ZnO could inhibit the crystal growth of BiOI.

To understand the component of these pure BiOI and ZnO-BiOI samples clearly, the total amount of ZnO coupling with BiOI was determined by WDXRF and the results are shown in Table 1. It shows that each of the samples has similar composition and contains Zn and Bi. Thus, it can be concluded that the as-synthesized samples are devoid of any other impurity atoms. It can also be found that the atomic ratio of n_{Bi}/n_{Zn} was to be about 0.0, 0.96, 1.93, 2.86, 4.91, which is close to the experimental dopant concentration.

Table 1 Elemental composition and BET of the as-synthesized samples

Samples	Pure BiOI	ZB-1	ZB-2	ZB-3	ZB-5
Atomic ratio of n_{Bi}/n_{Zn}	0.0	0.96	1.93	2.86	4.91
S_{BET} / ($m^2 \cdot g^{-1}$)	7	18	18	17	16

Furthermore, the obvious changes can be seen in Barrett-Emmett-Teller (BET) surface of the as-synthesized pure BiOI and ZnO-BiOI, which are shown in Table 1. Comparing with the specific surface area of pure BiOI, the specific surface area of ZnO-BiOI samples have been enlarged, which may be suitable for increasing the photocatalytic activity of the ZnO-BiOI samples.

2.2 FESEM and HRTEM images of the samples

To describe the morphology of the as-synthesized samples, FESEM was carried out. Fig.2(a) shows the FESEM image of pure BiOI sample. It can be found that all the as-synthesized pure BiOI samples are composed of hollow structures with the diameters in

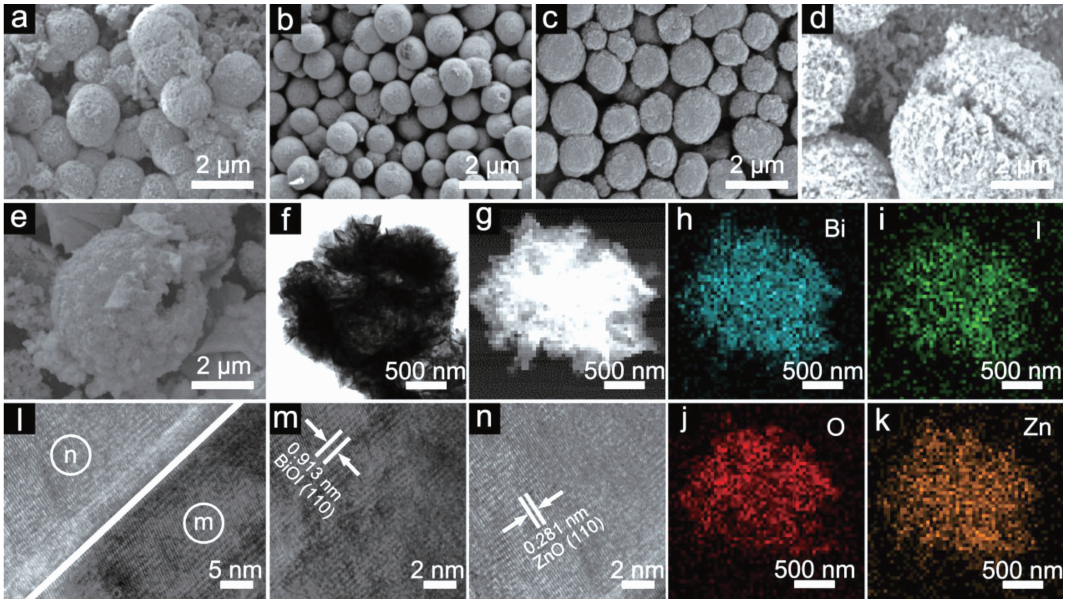

Fig.2 (a) FESEM images of pure BiOI; (b) FESEM images of ZB-1; (c) FESEM images of ZB-2; (d) FESEM images of ZB-3; (e) FESEM images of ZB-5; (f) HRTEM images of ZB-1; (g~k) HRSTEM-EDS mapping results o of ZB-1,(l~n) HRTEM images of ZB-1

the range of 2~3 mm, which is assembled by a large amount of nanoparticles. The morphology of ZnO with various ZnO coupling were also investigated by the FESEM and shown in Fig.2(b)~(e). Further increasing ZnO coupling with BiOI, the morphology of the spheres is rarely changed, a porous structure still exists with internal size of pores remaining unchanged. To confirm that as-synthesized ZB-1 sample has the uniform structure, the composition analyses of the ZB-1 sample were characterized by high-resolution electron microscopy (HREM) energy dispersive X-ray spectroscopy (EDS) mapping (scanning model of HRTEM) using a FEI F30 microscope equipped with an energy dispersive X-ray analysis (EDAX; FEI Company) energy EDS. High-resolution scanning transmission electron microscopy (HRSTEM) EDS mapping results in Fig.2(h)~(k) of the as-synthesized ZB-1 sample revealed that the composition of the sample contains Bi,I,O and Zn. further demonstrating the high purity of the ZnO and BiOI. Fig.2(l) reveals the highly crystalline nature as well as the different compositions of the ZB-1 heterostructure with different lattice fringe parameters,which also indicates the formation of a core/shell structure and close connection of the two crystalline materials. Fig.2 (n) shows a lattice spacing of 0.281 nm, which corresponds to the (110) plane of ZnO in the wurtzite phase. Fig.2(m) exhibits a lattice fringe spacing of 0.913 nm, which match well with the interplanar distances of the (110) plane of BiOI.

2.3 Characterization of as-prepared samples

UV-Vis diffuse reectance spectra of BiOI, ZnO and ZnO/BiOI microspheres are shown in Fig.3. Pure ZnO has almost no absorbance in the visible light range, with an absorbance edge of about 400 nm, where as pure BiOI has strong absorbance in the visible light range, with an absorbance edge around 660 nm (Fig.3(a)). In contrast, the ZnO/BiOI microspheres have prominent absorbance in the visible light range, and their edges range are between 620 and 660 nm. Fig.3(b) shows the representative photoluminescence (PL) spectra of the as-prepared samples with the excitation wavelength of 325 nm at room temperature. There are two peaks in undoped ZnO: one is the UV near-band-edge (NBE) emission centered at 375 nm; the other is a broad green region centered at 580 nm. Compared with that of pure ZnO, the emission of ZnO/BiOI microspheres is dramatically reduced. It might also suggest that the green emission of the as-synthesized ZnO/BiOI samples may be attributed to oxygen vacancies defects at the surface or in the bulk, indicating the decreased recombination of photo-generated holes with the electrons in intrinsic or extrinsic defects after photo irradiation process, which will enhance the photocatalytic efficiency.

The chemical composition and surface chemical states of the ZnO/BiOI heterostructures were further investigated by X-ray photoelectron spectroscopy (XPS). The peak positions in all of the XPS spectra were calibrated with C1*s* at 284.60 eV. The typical survey XPS spectrum of the ZnO/BiOI heterostructure (ZB-1) indicates that the product consists of Zn, Bi, O and I elements (Fig.3(c)). Two symmetric peaks at 1 022.1 and 1 045.2 eV in the high-resolution XPS spectrum of Zn2*p* are assigned to Zn2$p_{3/2}$ and Zn2$p_{1/2}$, indicating the existence of Zn^{2+} in the ZnO/BiOI heterostructure (Fig.3(d))[25]. Two strong peaks at 159.5 and 164.8 eV shown in Fig.3e are attributed to Bi4$f_{7/2}$ and Bi4$f_{5/2}$, respectively, which are characteristic of Bi^{3+} in BiOI. The satellite peaks with a distance of 1.8 eV between Bi4$f_{7/2}$ and Bi4$f_{5/2}$ main peaks are consistent with the reported values [24,26]. The O1*s* peaks for the ZnO/BiOI heterostructure (Fig.3f) can be deconvoluted into three peaks at 529.8, 532.5, and 533.8 eV, which correspond to the Bi-O bonds in [Bi_2O_2] slabs of the BiOI layered structure[27], the Zn-O bonds of ZnO[28], and the O-H bonds of the surface-adsorbed water [29], respectively. As for the high-resolution I3*d* XPS spectrum (Fig.3(g)), two peaks at 618.9 and 630.5 eV are associated with I3$d_{3/2}$ and I3$d_{5/2}$. Respectively, it is in good agreement with those in BiOI [24]. All of these results further conrm the coexistence of ZnO and BiOI in the ZnO/BiOI heterostructure.

Generally, semiconductor photocatalysis involves the generation of electrons in the conduction band and

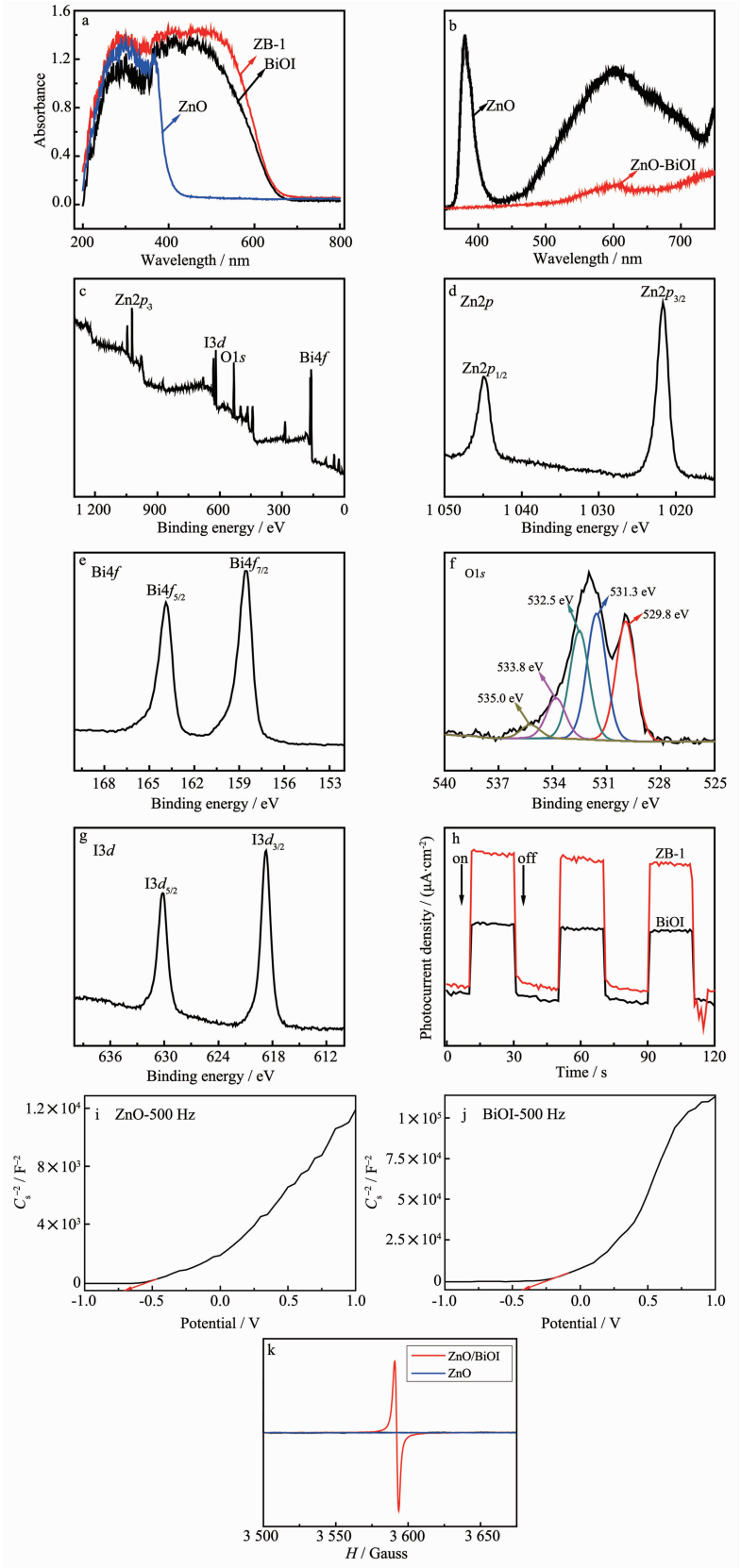

Fig.3 (a) DRS and (b) PL spectra of ZnO and ZnO/BiOI microspheres; XPS spectra of the ZnO-BiOI (c) the scan (d) Zn2*p* (e) Bi4*f* (f) O1*s* (g) I3*d*; (h) Transient photocurrent response for BiOI microspheres and ZB-1 microspheres under visible light irradiation,Mott-Schottky plots of (i) ZnO and (j) BiOI, (k) EPR spectra of ZnO, BiOI and ZnO/BiOI

holes in the valence band within a semiconductor upon light irradiation at energies equal to or greater than the band gap of the semiconductor. Subsequently, the utilization of photoexcited charge carriers to initiate redox reactions with suitable substrates on the semiconductor surface. To further understand the heterojunction effect on the photocatalytic activity enhancement of ZnO-BiOI microspheres, we carefully studied the photoinduced charge transfer properties of the ZnO-BiOI microspheres. It is known that the higher photocurrent intensity, the more effective the photo-induced carriers will separate. As shown in Fig.3 (h), the photocurrent intensity of the ZnO-BiOI microspheres is higher than that of BiOI microspheres, indicating that the ZnO-BiOI microspheres has a more effective separation of photo-induced electrons and holes and faster interfacial charge transfer, hence a higher photocatalytic activity.

BiOI has the smallest slope suggesting that the greatest current carrier density may lead to the most charge carriers involved into the reaction. As shown in Fig.3i ~3j, therefore, the at-band potentials (E_b) are −0.73 and −0.37 V (vs SCE) for ZnO and BiOI, respectively, which can be converted to −0.49 and −0.13 V (vs NHE). In addition, another important parameter is the at-band potential (E_b) conduction band (CB) values can be estimated from the E_b values, In generally, the conduction band (CB) position of n-type semiconductor is 0.1 ~0.3 V higher than the at-band potential[30-31]. The CB for ZnO and BiOI are −0.59 and −0.23 eV, respectively. The more positive the E_b value is, the greater the band bending is and the greater the barrier is for the corresponding semiconductor electrode in the reaction process. According to the above conclusion, their valence band positions can be calculated to be 2.62 and 1.80 V, respectively.

For a better understanding of the presence of oxygen vacancies in the lattice, we also recorded electron paramagnetic resonance (EPR) spectra (Fig.3 (k)). The EPR spectrum of ZnO displayed a resonance with good symmetry, which is attributed to the presence of an oxygen vacancy. The sharper and higher peak further confirmed that the existing oxygen vacancy in the crystal lattices of ZnO/BiOI samples has higher activity than ZnO. Therefore, the wavy line might indicate an increase in shallow defects in ZnO/BiOI, such as oxygen vacancies, which can absorb more oxygen molecules from the atmosphere. Meanwhile, when the unpaired electron was suppressed by the environment of the ions, such as detection temperature and the chemical status of adjacent ions, the signals could be broader. In this case, we also presumed that ZnO/BiOI was present on the surface which led to the broader line. This proved that the ZnO/BiOI sample has more stable oxygen vacancies in the lattices than the ZnO sample.

2.4 Photoctalytic performance of ZnO-BiOI porous microspheres

The possible schematic diagram for ZnO-BiOI photocatalytic degradation of RhB under visible light irradiation is shown in Scheme 1. Moreover, it can also be seen in BET surface, UV-visible spectra and potocurrent spectra of the as-synthesized ZnO-BiOI samples that the enhanced photocatalytic activity of ZnO-BiOI can also be attributed to the surface area

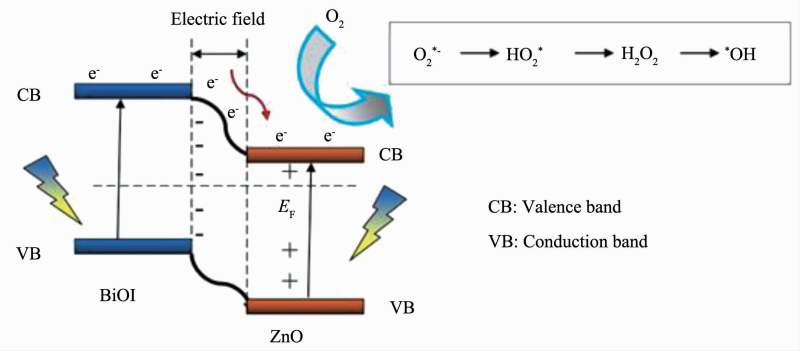

Scheme 1　Possible schematic diagram for ZnO-BiOI photocatalytic degradation of RhB under visible light irradiation

enlarged, excitonic peaks higher, the photoinduced electrons enhanced and holes separation of the ZnO-BiOI sample.

The photogenerated electrons would migrate from BiOI to the CB of ZnO. However, the VB potential of BiOI is higher than that of ZnO, so holes can only stay on the surface of BiOI. Furthermore, the internal electric eld can promote the separation of the electron. hole pairs, causing the electrons to move across the interface to the region of ZnO and the holes to transfer to the surface. Because the diffusion coeffcients for excess electrons and holes are different. The possible photocatalytic reaction process can be proposed as follows:

$$((BiOI/ZnO)+h\nu \rightarrow BiOI(\oplus)/ZnO(\ominus)$$

$$ZnO(\ominus)+O_2 \rightarrow ZnO+O_2\cdot^-$$

$$O_2\cdot^-+H_2O \rightarrow OH^-+HO_2\cdot$$

$$HO_2\cdot+H_2O \rightarrow 3OH\cdot$$

$$OH\cdot+RhB \rightarrow products$$

$$BiOI(\oplus)+RhB \rightarrow products$$

This suggests that the heterojunctions at the interface between BiOI and ZnO can greatly reduce the recombination of electron.hole pairs and extend the lifetime of charge carriers, which is another factor in the superior photocatalytic activity of ZnO/BiOI heterostructures in addition to high surface area.

The photocatalytic activities of as-fabricated products were evaluated by measuring CO_2 evolution from the photocatalytic decomposition of acetaldehyde. Fig.4 shows the time course of CO_2 liberation of samples with different amounts of original materials. Fig.4(a) shows Pure ZnO had a weak visible-light photocatalytic activity after 24 h of visible-light irradiation. Photocatalytic activities were enhanced by

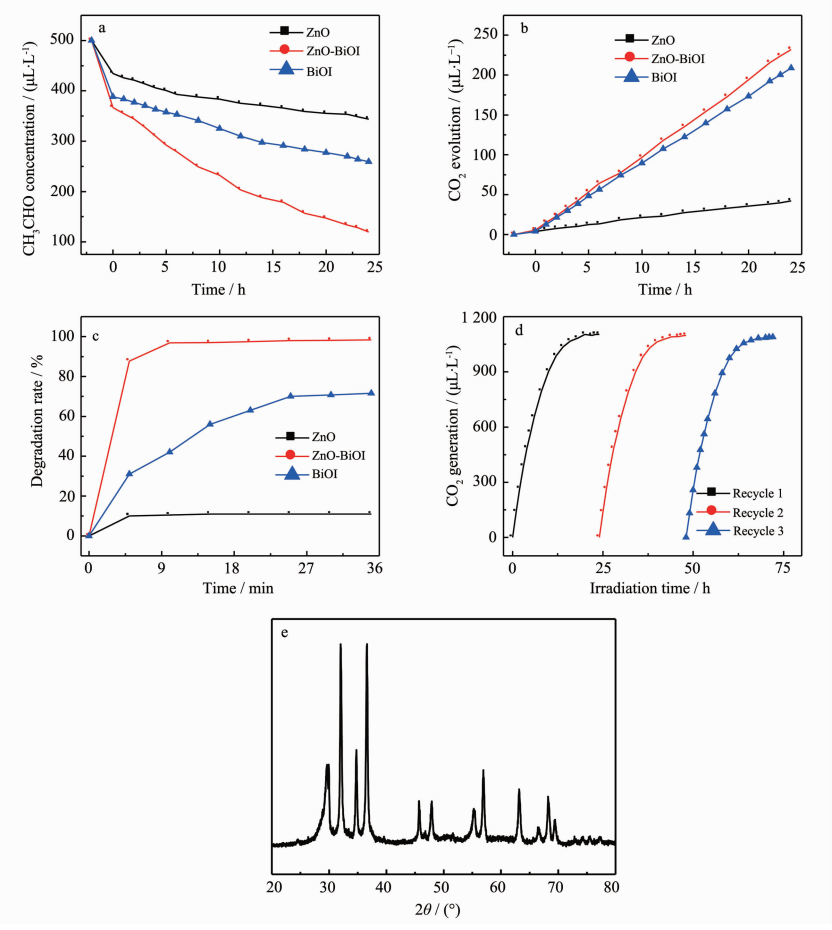

(a) CH_3CHO concentration; (b) CO_2 generation; (c) RhB degradation; (d) three recycles of CH_3CHO photodegradation evaluation by the ZB-1; (e) XRD pattern of ZnO-BiOI microspheres after photodegradation

Fig.4 Photocatalytic performance evaluation curves of the as-prepared photocatalysts

increasing the ZnO, and photocatalytic activity was higher than that of pure BiOI, the photocatalytic activities decreased. Change in photocatalytic activities can be attributed to the change in morphology (Fig.4b). Only the sample with porous ZnO/BiOI microspheres morphology had a higher concentration of oxygen vacancies than pure ZnO and pure BiOI owing to that porous ZnO/BiOI microspheres three dimensional hierarchical structure has a larger specific surface area and more activity oxygen exists on higher specific surface area. Besides, the photodegradation experiments of RhB aqueous solution were further carried out to investigate the universality of this heterojunction photocatalyst. Obviously, the RhB dyes photodegradation results in solution in Fig.4 (c) present a similar tendency with CH_3CHO ones in gaseous phase. In summary, this *in situ* prepared Porous ZnO/BiOI microspheres is with excellent photodegradation performance in RhB dye and CH_3CHO gas under visible light irradiation.

We also evaluated the stability and reusability of the ZnO/BiOI heterostructure (ZB-1). As shown in Fig. 4(d), no marked change in the photocatalytic activity was observed after three cycles of photodegradation, suggesting the good stability of the ZnO/BiOI heterostructures.In order to investigate the stability of the photocatalysts, The XRD patterns of this photocatalyst was also tested and shown in Fig.4 (e). The results indicated that this photocatalyst exhibits a good cycling stability.

3 Conclusions

In summary, we reported porous ZnO/BiOI microspheres that were synthesized though a simple method. The products were characterized by XRD, FESEM, HRTEM, PL and UV-Vis. The photocatalytic activity was explored by degradation of RhB dye and CH_3CHO gas. The photocatalytic results show that ZnO/BiOI microspheres can enhance the photocatalytic efficiency of ZnO under visible light irradiation. We can draw a conclusion that ZnO/BiOI microspheres porous hierarchical structure has a higher concentration of oxygen vacancies that results in enhancement of catalytic activity.

Acknowledgment: We gratefully acknowledge nancial support from the National Natural Science Foundation of China (No.21505118), the Natural Science Foundation of Jiangsu Province (No.BK2150438), Qing Lan project of Jiangsu Province (2016-15) and Yangzhou Polytechnic Institute key project (No. 2016xjzk001).

References:

[1] Mukhopadhyay S, Das P P, Maity S, et al. *Appl. Catal. B*, **2015**,**165**:128-138

[2] Umar A, Akhtar M S, Al-Hajry A, et al. *Chem. Eng. J.*, **2015**, **262**:588-596

[3] Chen Y, Zhao H, Liu B, et al. *Appl. Catal. B*, **2015**,**163**:189-197

[4] Tian C, Zhang Q, Wu A, et al. *Chem. Commun*., **2012**,**48**: 2858-2860

[5] Zhang H J, Chen G H, Bahnemann D W. *J. Mater. Chem.*, **2009**,**19**:5089-5121

[6]Kayaci F, Vempati S, Ozgit-Akgun C, et al. *Appl. Catal. B*, **2014**,**156-157**:173-183

[7] Wahab R, Tripathy S K, Shin H S, et al. *Chem. Eng. J.*, **2013**, **226**:154-160

[8]Pan L K, Liu X J, Sun Z, et al. *J. Mater. Chem. A*, **2013**,**1**: 8299-8326

[9]Wu C L. *Appl. Surf. Sci.*, **2014**,**319**:237-243

[10]Lai Y L, Meng M, Yu Y F, et al. *Appl. Catal. B*, **2011**,**105**: 335-345

[11]Kochuveedu S T, Jang Y H, Kim D H. *Chem. Soc. Rev.*, **2013**, **42**:8467-8493

[12]Sun S, Wang W, Zeng S, et al. *J. Hazard. Mater.*, **2010**,**178**: 427-433

[13]Zhang X L, Zhao J L,Wang S G, et al. *Int. J. Hydrogen Energy*, **2014**,**39**:8238-8245

[14]Ai Z, Huang Y, Lee S, Zhang L. *J. Alloys Compd*., **2011**, **509**:2044-2049

[15]Kibanova D, Sleiman M, Cervini-Silva J, et al. *J. Hazard. Mater.*, **2012**,**211-212**:233-239

[16]Liao Y C, Xie C S, Liu Y, et al. *Ceram Int*., **2012**,**38**:4437-4444

[17]Tian H, He J H, Liu L L, et al. *Microporous Mesoporous Mater.*, **2012**,**151**:397-402

[18]Yang L P, Liu Z Y, Shi J W, et al. *Sep. Purif. Technol.*, **2007**, **54**:204-211

[19]You Y, Zhang S Y, Wan L, Xu D F. *Appl. Surf. Sci.*, **2012**,

258:3469-3474

[20]Zhang L, Fu H, Zhang C, et al. *J. Solid State Chem.*,**2006**, **179**:804-811

[21]Zhou J, Mullins D R. *Surf. Sci.*, **2006**,**600**:1540-1546

[22]ZhuY, Yu F, Man Y, et al. *J. Solid State Chem.*, **2005**,**178**: 224-229

[23]Wang Y Y, Zhou G Q, Guo J, et al. *Ceram Int.*, **2016**,**42**: 12467-12474

[24]Zhang X, Zhang L Z, Xie T F, et al. *J. Phys. Chem. C*, **2009**,**113**:7371-7378

[25]Chang Y G, Xu J, Zhang Y Y, et al. *J. Phys. Chem. C*, **2009**, **113**:18761-18767

[26]Gurunathan K. Int. *J. Hydrogen Energy*, **2004**,**29**:933-940

[27]Zhang K L, Liu C M, Huang F Q, et al. *Appl. Catal. B*, **2006**, **68**:125-129

[28]Jiang J, Zhang X, Sun P B, et al. *J. Phys. Chem. C*,**2011**, **115**:20555-20564

[29]Coppa B J, Davis R F, Nemanich R J. *Appl. Phys. Lett.*, **2003**, **82**:400-402

[30]Moniz S J, Tang J. *ChemCatChem*, **2015**,**7**:1659-1667

[31]Chun W J, Ishikawa A, Fujisawa H, et al. *J. Phys. Chem. B*, **2003**,**107**:1798-1803